

Spacecraft Attitude Estimation and Sensor Calibration Using Moving Horizon Estimation

Jeroen Vandersteen,^{*} Moritz Diehl,[†] Conny Aerts,[‡] and Jan Swevers[§]
Katholieke Universiteit Leuven, BE-3001 Leuven, Belgium

DOI: 10.2514/1.58805

This paper presents the real-time moving horizon estimation of a spacecraft's attitude and sensor calibration parameters, applied to two space mission scenarios. In the first scenario, the attitude is estimated from three-axis magnetometer and gyroscope measurements. In the second scenario, a star tracker is used to jointly estimate the attitude and gyroscope calibration parameters. A moving horizon estimator determines the current states and parameters by solving a constrained numerical optimization problem, considering a finite sequence of current and past measurement data, an available dynamic model and state constraints. The objective function to be minimized is typically a tradeoff between minimizing measurement noise, process noise, and an initial cost. To solve this constrained optimization problem in real time, an efficient numerical solution method based on the iterative Gauss–Newton scheme has been implemented and specific measures are taken to speed up the calculations by exploiting the sparsity and band structure of matrices to be inverted. Numerical simulation is used to verify that the proposed method results in a faster convergence from large initialization errors and an increased accuracy on nonlinear systems with respect to extended Kalman filtering.

I. Introduction

IN THIS work, moving horizon estimation (MHE) is applied to spacecraft attitude estimation. Attitude estimation is the technique used to determine the orientation of a spacecraft with respect to a reference coordinate frame, based on onboard sensors. A gyroscope (or gyro) is commonly used onboard spacecraft to measure the angular velocity of the spacecraft. The output of the gyro is subject to measurement bias. The effect of the gyro bias can be offset by a sensor that directly measures the attitude. A single three-axis magnetometer (TAM) measures the geomagnetic field vector and provides only two axes of attitude information. The roll angle around this vector observation cannot be resolved. Three-axis attitude can be determined as the geomagnetic field vector changes direction over an orbit. This attitude determination process is complicated by the nonlinear equations governing the spacecraft kinematics and measurements. Both the gyroscope and the TAM measurements are corrupted by measurement noise. Previous research has focused on the effects of nonlinearities (in both the measurement model and the plant model) and on convergence from large initial errors. Basic work on this subject is summarized by Lefferts et al. [1] and Markley [2]. A survey of existing algorithms for nonlinear attitude estimation is given in [3]. A multiplicative extended Kalman filter (MEKF) based on vector observations has been developed by Psiaki et al. [4]. This filter yields good results in the linear regime, when initialized with small errors. For large initial errors, the propagated and updated covariances are not a good representation of the actual estimation covariance and may cause the MEKF to diverge from the actual

states. A second-order Kalman filter has been developed to avoid prolonged convergence due to nonlinearities [5]. An unscented Kalman filter (UKF) has been developed to address this same issue [6]. The unscented filter makes use of a set of sigma points that are independently propagated through the nonlinear model, and the resulting covariance is updated with the measurement function. The propagated and updated covariances are then computed from the statistical ensemble of the updated sigma points. By making use of this unscented transform, the unscented Kalman filter is able to capture both first- and second-order terms of a nonlinear system, thereby potentially achieving a better estimation performance than the EKF for some nonlinear systems. The UKF represents the current state of the art in onboard attitude estimation as, for example, used in the project for on-board autonomy (PROBA)-2 space mission [7]. Particle filters (PF) have been developed to accurately capture the full a posteriori estimation error covariance [8,9]. They have extremely good convergence properties for this problem. However, the computational cost of particle filters currently inhibits their practical implementation on the onboard software of spacecraft.

The filters described in these previous works do not take sensor calibration into account because they assume that sensors are calibrated offline using batch estimation techniques, for example, described by Shuster et al. [10] for calibration of relative sensor misalignment, or techniques surveyed in [11]. Calibration errors, most notably the gyro scale factor and nonorthogonality errors, can have a detrimental effect on the accuracy of an attitude estimation filter, as shown by Pittelkau in [12]. In this latter work, a Kalman filter was developed to jointly estimate the attitude and gyro calibration parameters, which removes the need for offline calibration and increases the accuracy of the attitude estimator.

All of the preceding filters estimate the state at the current time based on a prior estimate and current measurement. However, for nonlinear systems, the prior probability density can, in general, only be estimated, resulting in a suboptimal state estimate. This may cause a loss in estimation efficiency (a deviation from the Cramér–Rao lower bound) or, in some cases, even the divergence of the filter from the true state vector. The moving horizon estimator attempts to overcome this problem by including a longer horizon of measurements into the estimation problem. This reduces the sensitivity of the estimator to the prior density and reduces the effect of incorrect initialization and propagation of the prior probability density. The estimated states are computed by minimizing a cost term that is typically a tradeoff between measurement noise, process noise, and a cost associated with a prior estimate of the states at the beginning of the horizon. This last cost will be named the “arrival cost,” because

Received 30 April 2012; revision received 1 August 2012; accepted for publication 2 August 2012; published online 12 February 2013. Copyright © 2012 by Jeroen Vandersteen. Published by the American Institute of Aeronautics and Astronautics, Inc., with permission. Copies of this paper may be made for personal or internal use, on condition that the copier pay the \$10.00 per-copy fee to the Copyright Clearance Center, Inc., 222 Rosewood Drive, Danvers, MA 01923; include the code 1533-3884/13 and \$10.00 in correspondence with the CCC.

^{*}Mechanical Engineer, Institute for Astronomy, Celestijnenlaan 200 D; currently AOCs Engineer at the European Space Agency (ESA), Keplerlaan 1, 2201 AZ Noordwijk, The Netherlands; Jeroen.Vandersteen@esa.int. Full Member AIAA.

[†]Professor, Department of Electrical Engineering, Kasteelpark Arenberg 10; Moritz.Diehl@esat.kuleuven.be.

[‡]Professor, Institute of Astronomy, Celestijnenlaan 200 D; Conny.Aerts@ster.kuleuven.be.

[§]Professor, Department of Mechanical Engineering, Celestijnenlaan 300 B; Jan.Swevers@mech.kuleuven.be.

this represents the cost to arrive at the initial point in the horizon. Using all the measurements since the beginning of the mission is impractical, therefore a finite horizon length N is chosen as a tradeoff between computational complexity and estimation convergence. The objective of MHE is to estimate the states and parameters over the entire estimation horizon N . In that sense, the MHE formulation is similar to batch state estimation algorithms, such as fixed-interval and fixed-lag smoothers. Early work on the application of smoothers to state and parameter estimation for linear systems was done by Rauch et al. [13], Moore [14], and Elliot and Moore [15]. It has been shown in [16] that smoothing has an improvement on filtering for parameter estimation problems. However, most smoothers operate on a linear model, in which case the smoother reduces to a forward-backward filter with Kalman updates, such as the smoother presented in [13]. In the linear case, the smoothed state estimate at the final time step is exactly the same as the filtered state estimate at that time instant. The solution of the MHE, however, is in general different from the filtered and smoothed estimates for nonlinear systems. Smoothing has been extended to nonlinear systems by Moore and Tam [17]. The fundamental difference between a nonlinear smoother and the MHE is the explicit treatment of constraints (equality, inequality, or both) in the optimization problem. An interesting algorithm for sensor calibration of the TOPEX/Poseidon space mission, similar to MHE, is presented in [18]. In that algorithm, the estimation of the calibration parameters is performed by solving an unconstrained recursive least-squares problem and can operate on a sliding window and incorporate prior state information. As opposed to MHE, parameters and states are not jointly estimated. Rather, a separate loop is used to estimate each. Smoothing is often used to obtain an estimated attitude history for postflight analysis (see, for example, [19,20]).

Early work on MHE was done by Ohtsuka and Fujii [21], Rao et al. [22], and Tenny and Rawlings [23]. A globally convergent MHE algorithm is presented in [24] (not yet real-time feasible, however) and in [25] for linear systems. In [26], an algorithm based on backward single shooting is presented, along with a comprehensive stability analysis. Only very recently, real-time algorithms for MHE with very short sampling times have been presented by Zavala et al. [27] and Kühl et al. [28]. The latter work describes a real-time iteration (RTI) algorithm for MHE. In this RTI algorithm, the MHE problem is initialized with the previous solution and the computation of the current solution is limited to a single Gauss-Newton iteration. It is then possible to derive an upper bound on the necessary computation time, which fulfills the formal requirement of real-time implementation.

If the MHE problem is formulated as a numerical least-squares optimization problem, many existing numerical optimization methods can be used to find a solution. Numerical optimization methods are described in [29], and in [30] for MHE specifically. Numerical methods for parameter estimation in nonlinear systems described by differential-algebraic equations are presented in [31]. In particular, the use of “multiple shooting” to discretize the continuous-time problem into a boundary value problem is described. In this paper, an MHE with only equality constraints is developed, which will lead to an efficient solution method that makes the real-time implementation of the MHE in the onboard software of spacecraft possible.

The contribution of this work to the field of spacecraft attitude determination is to introduce the concept of moving horizon estimation and to apply it to two common problems encountered in spacecraft operations. To achieve real-time estimation given limited onboard computing resources, several measures to speed up the calculations are implemented, such as exploiting the sparsity and band structure of the matrices to be inverted and hot starting from a previous solution. Furthermore, a method to compute the arrival covariance without requiring additional computations is developed.

This paper is structured as follows. Section II describes the MHE formulation in more detail, as well as the solution method based on consecutive Gauss-Newton iterations. A reordering method is presented, as well as the RTI implementation of MHE. The developed moving horizon estimator is applied to the problem of spacecraft attitude estimation from three-axis magnetometer and gyroscope measurements in Sec. III. The performance of the MHE is compared

with extended and unscented Kalman filtering and particle filtering using numerical simulation. Section IV describes an example problem where the gyrosensor nonorthogonality and scale factor calibration parameters are estimated with the spacecraft attitude. The performance of the MHE is compared with different versions of the extended Kalman filter and an augmented Kalman filter. Finally, this paper ends with some general conclusions in Sec. V.

II. Moving Horizon Estimation with Equality Constraints

This section describes a solution strategy to solve a general moving horizon estimation problem through successive linearization. This method will be applied to spacecraft attitude estimation in the following two sections. For convenience of notation, in the remainder of this paper, the time indices are redefined so that the measurement horizon always starts with index 1 and ends with index N without loss of generality. Time index N then always denotes the current time. The MHE problem is here defined as follows:

$$\begin{aligned} & \text{minimize} \quad \frac{1}{2} \sum_{i=2}^N \nu_i^T R_i^{-1} \nu_i + \frac{1}{2} \sum_{i=1}^{N-1} \omega_i^T Q_i^{-1} \omega_i \\ & x_1, \dots, x_N \\ & \nu_2, \dots, \nu_N \\ & \omega_1, \dots, \omega_{N-1} \\ & + \frac{1}{2} (x_1^{(-)} - x_1)^T (P_1^{(-)})^{-1} (x_1^{(-)} - x_1) \end{aligned} \quad (1)$$

subject to

$$x_{i+1} = f(x_i, u_i) + \omega_i \quad \text{for } i = 1, \dots, N-1 \quad (2)$$

$$y_i = h(x_i) + \nu_i \quad \text{for } i = 2, \dots, N \quad (3)$$

$$L_i(x_i) = 0 \quad \text{for } i = 1, \dots, N \quad (4)$$

where x_i are the states to be estimated, with Eq. (2) describing the state propagation in discrete time. In this propagation equation, u_i are the known inputs, with process noise ω_i and process noise covariance Q_i . Equation (3) describes the measurement equation, with y_i the measurements, ν_i the measurement noise, and R_i the measurement noise covariance. The estimate at the first time point in the horizon is $x_1^{(-)}$, with covariance $P_1^{(-)}$. The third term in the cost function thus describes the arrival cost. Note that the measurement at time point $i = 1$ is not included in the cost function. It is assumed that all the information from this measurement is already contained in the prior estimate $x_1^{(-)}$. The equality constraints are given by Equation 4. The output of the MHE is then x_N : the estimated state vector at the final point in the horizon. In this paper, it is assumed that no inequality constraints are present. This is thus a weighted least-squares problem, in which the weights are the inverse of the covariance matrices:

$$W_{m,i} = R_i^{-1} \quad (5)$$

$$W_{p,i} = Q_i^{-1} \quad (6)$$

$$W_a = (P_1^{(-)})^{-1} \quad (7)$$

We adopt the following notation:

$$[a]^T W[a] = \|a\|_W^2 \quad (8)$$

When substituting the state propagation Eq. (2) and measurement Eq. (3) in the cost function (1), we obtain the following alternative formulation:

$$\begin{aligned} \underset{x_i}{\text{minimize}} \quad & \frac{1}{2} \sum_{i=2}^N \|y_i - h(x_i)\|_{W_{m,i}}^2 + \frac{1}{2} \sum_{i=1}^{N-1} \|x_{i+1} - f(x_i, u_i)\|_{W_{p,i}}^2 \\ & + \frac{1}{2} \|x_1^{(-)} - x_1\|_{W_a}^2 \end{aligned} \quad (9)$$

subject to

$$l_i(x_i) = 0 \quad \text{for } i = 1, \dots, N \quad (10)$$

This nonlinear least-squares problem is solved using an iterative Gauss–Newton solution method. In each iteration, the measurement and state propagation functions are linearized about the previous solution \bar{x}_i (or the best estimate, if no previous solution is available), with $\Delta x_i = x_i - \bar{x}_i$ the deviation from this nominal state:

$$\begin{aligned} \underset{\Delta x_i}{\text{minimize}} \quad & \frac{1}{2} \sum_{i=2}^N \left\| y_i - h(\bar{x}_i) - \frac{\partial h(\bar{x}_i)}{\partial x_i} \Delta x_i \right\|_{W_{m,i}}^2 \\ & + \frac{1}{2} \sum_{i=1}^{N-1} \left\| \bar{x}_{i+1} - f(\bar{x}_i, u_i) + \Delta x_{i+1} - \frac{\partial f(\bar{x}_i, u_i)}{\partial x_i} \Delta x_i \right\|_{W_{p,i}}^2 \\ & + \frac{1}{2} \|x_1^{(-)} - \bar{x}_1 - \Delta x_1\|_{W_a}^2 \end{aligned} \quad (11)$$

subject to

$$l_i(\bar{x}_i) + \frac{\partial l(\bar{x}_i)}{\partial x_i} \Delta x_i = 0 \quad \text{for } i = 1, \dots, N \quad (12)$$

By introducing the state deviation trajectory over the entire horizon $\Delta X = [\Delta x_1^T, \Delta x_2^T, \dots, \Delta x_N^T]^T$, this optimization problem is rewritten as

$$\begin{aligned} \underset{\Delta X}{\text{minimize}} \quad & \frac{1}{2} \|A_m \Delta X - B_m\|_{W_m}^2 + \frac{1}{2} \|A_p \Delta X - B_p\|_{W_p}^2 \\ & + \frac{1}{2} \|A_a \Delta X - B_a\|_{W_a}^2 \end{aligned} \quad (13)$$

subject to

$$A_{\text{eq}} \Delta X - B_{\text{eq}} = 0 \quad (14)$$

where the matrices and vectors related to the measurement cost are

$$A_m = \text{diag} \left(-\frac{\partial h(\bar{x}_2)}{\partial x_2}, -\frac{\partial h(\bar{x}_3)}{\partial x_3}, \dots, -\frac{\partial h(\bar{x}_N)}{\partial x_N} \right) \quad (15)$$

$$B_m = [(h(\bar{x}_2) - y_1)^T, (h(\bar{x}_3) - y_2)^T, \dots, (h(\bar{x}_N) - y_N)^T]^T \quad (16)$$

$$W_m = \text{diag}(R_2^{-1}, R_3^{-1}, \dots, R_N^{-1}) \quad (17)$$

The matrices and vectors related to the state propagation cost are

$$A_p = \begin{bmatrix} -\frac{\partial f(\bar{x}_1, u_1)}{\partial x_1} & 1 & 0 & \dots & 0 \\ 0 & -\frac{\partial f(\bar{x}_2, u_2)}{\partial x_2} & 1 & \dots & 0 \\ & & \ddots & & \\ 0 & 0 & \dots & -\frac{\partial f(\bar{x}_{N-1}, u_{N-1})}{\partial x_{N-1}} & 1 \end{bmatrix} \quad (18)$$

$$B_p = [(f(\bar{x}_1, u_1) - \bar{x}_2)^T, (f(\bar{x}_2, u_2) - \bar{x}_3)^T, \dots, (f(\bar{x}_{N-1}, u_{N-1}) - \bar{x}_N)^T]^T \quad (19)$$

$$W_p = \text{diag}(Q_1^{-1}, Q_2^{-1}, \dots, Q_{N-1}^{-1}) \quad (20)$$

and one is the identity matrix. The matrices and vectors related to the arrival cost are

$$A_a = [-1, 0, \dots, 0] \quad (21)$$

$$B_a = [\bar{x}_1 - x_1^{(-)}] \quad (22)$$

$$W_a = (P_1^{(-)})^{-1} \quad (23)$$

Finally, the matrices and vectors related to the equality constraints are

$$A_{\text{eq}} = \text{diag} \left(\frac{\partial l_1(\bar{x}_1)}{\partial x_1}, \frac{\partial l_2(\bar{x}_2)}{\partial x_2}, \dots, \frac{\partial l_N(\bar{x}_N)}{\partial x_N} \right) \quad (24)$$

$$B_{\text{eq}} = [-l(\bar{x}_1)^T, -l(\bar{x}_2)^T, \dots, -l(\bar{x}_N)^T]^T \quad (25)$$

The linearized cost function in Eq. (13) can then be combined into

$$\begin{aligned} J(\Delta X) = & \frac{1}{2} \Delta X^T (A_m^T W_m A_m + A_p^T W_p A_p + A_a^T W_a A_a) \Delta X \\ & - (A_m^T W_m B_m + A_p^T W_p B_p + A_a^T W_a B_a) \Delta X + \frac{1}{2} C \end{aligned} \quad (26)$$

$$= \frac{1}{2} [\Delta X^T \Delta X - 2G \Delta X + C] \quad (27)$$

with C being a constant matrix, and G defined by the corresponding terms in Eqs. (26) and (27). This results in a least-squares objective function with linear constraints. This constrained linear-least-squares problem can be solved by introducing a vector of Lagrange multipliers $\Lambda = [\lambda_1^T, \lambda_2^T, \dots, \lambda_N^T]^T$ and constructing the Karush–Kuhn–Tucker (KKT) matrices [32] as

$$\mathcal{J} = \begin{bmatrix} A_{\text{eq}} & A_{\text{eq}}^T \\ 0 & 0 \end{bmatrix} \quad (28)$$

$$F = \begin{bmatrix} G \\ B_{\text{eq}} \end{bmatrix} \quad (29)$$

The solution of this optimization problem can be found as

$$\begin{bmatrix} \Delta X \\ \Lambda \end{bmatrix} = \mathcal{J}^{-1} F \quad (30)$$

The solution of this optimization problem requires only one matrix factorization, as seen in Eq. (30). From Eqs. (15), (18), (24), and (26), it can be seen that the matrices A_{eq} and A_{eq} have a band-diagonal structure. However, from Eq. (28) it is clear that the matrix \mathcal{J} that needs to be factorized does not have this band-diagonal structure. If the variables are reordered from $[\Delta X^T, \Lambda^T]^T = [\Delta x_1^T, \Delta x_2^T, \dots, \Delta x_N^T, \lambda_1^T, \lambda_2^T, \dots, \lambda_N^T]^T$ to $Z = [\Delta x_1^T, \lambda_1^T, \Delta x_2^T, \lambda_2^T, \dots, \Delta x_N^T, \lambda_N^T]^T$, the \mathcal{J} matrix does preserve this band-diagonal structure. The effect on the structure of the \mathcal{J} matrix is illustrated in Fig. 1. This band-diagonal matrix structure can be exploited by using efficient algorithms to factorize the \mathcal{J} matrix much faster than a full matrix. The computation time to solve the linearized system does not scale more than linearly with the horizon length. If the weight matrices W_m , W_p , and W_a are chosen to be the inverse of the actual covariance matrices, it is well known that the upper left block of the inverse of the original \mathcal{J} matrix, as defined in Eq. (28), is equal to the linear estimation error covariance matrix for the state trajectory over the horizon (e.g., see [31]). Because the inverse of \mathcal{J} needs to be

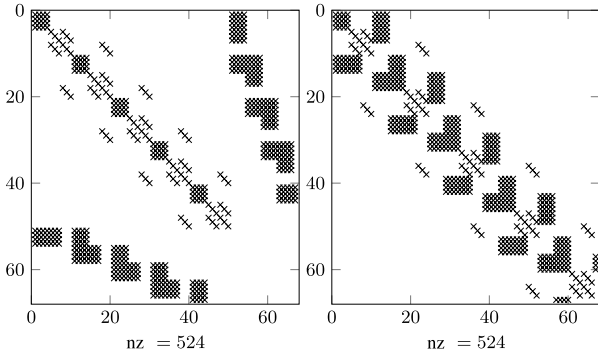


Fig. 1 Nonzero elements in the KKT matrix: without reordering (left panel) and with reordering (right panel).

computed to solve the MHE problem, the linear estimation error covariance is simultaneously computed without additional numerical operations. This linear estimation error covariance can be stored for later use as the arrival cost in future MHE solution steps. For an infinite measurement horizon length, the arrival cost term disappears in the MHE formulation. Hence, for a very long measurement horizon, the cost term may be omitted without significant loss of accuracy.

In the RTI MHE algorithm described by Kühl et al. in [28], the solution at the previous time is used to initialize the Gauss–Newton scheme. The oldest information is discarded, and the rest of the solution over the horizon is shifted one step backward in time and the state vector at the current time step is predicted using the available plant model. Then only one Gauss–Newton iteration is computed at each time step, instead of computing a fully converged MHE solution. This results in an MHE with a guaranteed maximum number of computations and thus guarantees an upper bound on the computation time, yielding a real-time estimator.

III. Attitude Estimation from Vector Observations

This section provides a first application of moving horizon estimation. The attitude of a space vehicle is to be estimated from three-axis magnetometer and gyroscope measurements. The nonlinear continuous-time models that are used are presented first. Then, a discretization method of the states over the horizon is developed. The application of MHE is described, and simulation results are used to verify the performance of the MHE.

A. Nonlinear Continuous-Time Model

The attitude of a rigid body in inertial space can be represented using many parameterization techniques, such as the Gibbs vector, Euler angles, Rodriguez parameters, the direction cosine matrix, or quaternion parameters. It has been shown that any three-element parameterization technique, such as Euler angles, suffers from a singularity known as Gimbal lock [33]. To avoid this problem, the four-element quaternion is widely adopted by the aerospace industry. The quaternion vector q is defined as [33]

$$q = \begin{bmatrix} q_1 \\ q_2 \\ q_3 \\ q_4 \end{bmatrix} \equiv \begin{bmatrix} e_x \sin(\alpha/2) \\ e_y \sin(\alpha/2) \\ e_z \sin(\alpha/2) \\ \cos(\alpha/2) \end{bmatrix} = \begin{bmatrix} q_{1:3} \\ q_4 \end{bmatrix} \quad (31)$$

where $e = [e_x, e_y, e_z]^T$ is the principal rotation axis and α is the corresponding rotation angle describing the rotation of a reference coordinate frame to the spacecraft body frame. The quaternion vector thus completely and unambiguously describes the orientation of a rigid body in the reference coordinate frame. From this definition, it can easily be seen that the quaternion vector must always obey a unit norm constraint: $\|q\| = 1$. Because a quaternion vector represents a rotation, the quaternion multiplication $q \otimes q'$ can be defined as the combined rotation of two quaternions q and q' :

$$q \otimes q' = \begin{bmatrix} q_4 & q_3 & -q_2 & q_1 \\ -q_3 & q_4 & q_1 & q_2 \\ q_2 & -q_1 & q_4 & q_3 \\ -q_1 & -q_2 & -q_3 & q_4 \end{bmatrix} \begin{bmatrix} q'_1 \\ q'_2 \\ q'_3 \\ q'_4 \end{bmatrix} \quad (32)$$

The error quaternion q_E , describing the rotation *from* one quaternion q' to another quaternion q , is then defined as

$$q_E = q^{-1} \otimes q' = \begin{bmatrix} -q_4 & -q_3 & q_2 & q_1 \\ q_3 & -q_4 & -q_1 & q_2 \\ -q_2 & q_1 & -q_4 & q_3 \\ q_1 & q_2 & q_3 & q_4 \end{bmatrix} \begin{bmatrix} q'_1 \\ q'_2 \\ q'_3 \\ q'_4 \end{bmatrix} = E(q)q' \quad (33)$$

The direction cosine matrix A (sometimes referred to as the attitude matrix) that corresponds to a quaternion q can be calculated as

$$A(q) = (q_4^2 - q_{1:3}^T q_{1:3}) 1_{3 \times 3} + 2q_{1:3} q_{1:3}^T - 2q_4 [q_{1:3} \times] \quad (34)$$

where the matrix $[q_{1:3} \times]$ is the skew-symmetric matrix describing the cross product and $1_{3 \times 3}$ is the 3×3 identity matrix. The attitude matrix corresponding to the multiplication of two quaternions is then equal to the multiplication of the attitude matrices of each of the individual quaternions:

$$A(q \otimes q') = A(q)A(q') \quad (35)$$

The kinematics describing the quaternion motion are given by

$$\dot{q} = \frac{1}{2} \begin{bmatrix} 0 & \omega_z & -\omega_y & \omega_x \\ -\omega_z & 0 & \omega_x & \omega_y \\ \omega_y & -\omega_x & 0 & \omega_z \\ -\omega_x & -\omega_y & -\omega_z & 0 \end{bmatrix} \begin{bmatrix} q_1 \\ q_2 \\ q_3 \\ q_4 \end{bmatrix} = \frac{1}{2} \Omega(\omega)q \quad (36)$$

$$= \frac{1}{2} \begin{bmatrix} q_4 & -q_3 & q_2 \\ q_3 & q_4 & -q_1 \\ -q_2 & q_1 & q_4 \\ -q_1 & -q_2 & -q_3 \end{bmatrix} \begin{bmatrix} \omega_x \\ \omega_y \\ \omega_z \end{bmatrix} = \frac{1}{2} \Xi(q)\omega \quad (37)$$

where $\omega = [\omega_x, \omega_y, \omega_z]^T$ are the angular rates, as seen in the body coordinate frame. These quaternion kinematics do not suffer from a singularity for any rotation.

The spacecraft is equipped with two sensors: a magnetometer, which provides vector observations, and a gyro, which provides angular rate measurements. The measurement model for the TAM at each discrete time i can be assumed to be of the form

$$b_i^m = A(q_i)r_i + \nu_i \quad (38)$$

where r_i is the geomagnetic field vector expressed in the reference coordinate frame, and b_i^m is this vector expressed in the spacecraft body frame of reference, with ν_i the zero-mean Gaussian measurement noise with covariance R_i . From a single TAM measurement, the attitude is not instantaneously observable. It is intuitive to understand that the roll angle around the observed vector cannot be resolved. If multiple vector sensors are present onboard the spacecraft, the attitude can be determined, provided the reference vectors are not collinear or nearly collinear. The second onboard sensor provides angular rate measurements, provided by gyroscopes. A simple, yet commonly used gyroscope model, is given by [33]

$$\omega^m(t) = \omega(t) + \beta(t) + \eta_o(t) \quad (39)$$

$$\dot{\beta}(t) = \eta_u(t) \quad (40)$$

where η_o is the gyro noise modeled as additive zero-mean Gaussian noise, and the gyro bias β is modeled as a random walk, with

$$E[\eta_v(t)\eta_v^T(\tau)] = 1_{3 \times 3} \sigma_v^2 \delta(t - \tau) \quad (41)$$

$$E[\eta_u(t)\eta_u^T(\tau)] = 1_{3 \times 3} \sigma_u^2 \delta(t - \tau) \quad (42)$$

B. Full Discretization of the Continuous-Time Dynamics

To use the proposed MHE formulation from Sec. II, the continuous-time dynamics are discretized over the measurement horizon. When using a numerical integrator to propagate the quaternion in time, the normalization constraint must not be violated. Simply integrating Eq. (36) will, in general, not yield a unit norm quaternion. Several methods exist to overcome this problem. A brute-force solution is using a normalization step after each integration step. Another technique involves propagating the local error vector and updating the quaternion. Here, a discrete-time symplectic integrator [34] that preserves the quaternion norm is used:

$$\left(1 - \frac{\Delta t}{4} \Omega(\omega_i)\right) \mathbf{q}_{i+1} = \left(1 + \frac{\Delta t}{4} \Omega(\omega_i)\right) \mathbf{q}_i, \quad \text{for all } i = 1, \dots, N-1 \quad (43)$$

From this last equation, the angular velocity vector can be computed from the quaternion trajectory:

$$\omega_i(\mathbf{q}_i, \mathbf{q}_{i+1}) = (\Xi(\mathbf{q}_i) + \Xi(\mathbf{q}_{i+1}))^{-1}(\mathbf{q}_{i+1} - \mathbf{q}_i), \quad \text{for all } i = 1, \dots, N-1 \quad (44)$$

This allows us to eliminate the states ω from the optimization problem and to drop the norm-preserving integration constraint (43) from the optimization problem. Because ω has only three components, whereas \mathbf{q} has four, we need to add the norm constraint on the quaternions at each time node to have a well-defined relation between \mathbf{q} and ω and to make sure that all quaternions remain of unit norm. For the bias drift, a simple forward Euler discretization is proposed:

$$\beta_{i+1} = \beta_i + \Delta t \dot{\beta}_i, \quad \text{for all } i = 1, \dots, N-1 \quad (45)$$

C. Moving Horizon Estimation Formulation

A moving horizon estimator has been developed to estimate the quaternions and gyro bias over the measurement horizon, where the last point ($i = N$) corresponds to the current time. The MHE is based on the idea that, by using a window of vector measurements, the problem is fully observable and less susceptible to incorrect initialization. The MHE problem formulation for attitude estimation from three-axis magnetometer and gyroscope measurements, is then

$$\begin{aligned} \text{minimize} \quad & \underbrace{\frac{1}{2} \left\| \begin{matrix} \mathbf{q}_1^{(-)} \\ \beta_1^{(-)} \end{matrix} - \begin{matrix} \mathbf{q}_1 \\ \beta_1 \end{matrix} \right\|_{W_a}^2}_{\text{arrival cost}} + \underbrace{\frac{1}{2} \sum_{i=2}^N \left\| \mathbf{b}_i^m - A(\mathbf{q}_i) \mathbf{r}_i \right\|_{W_m}^2}_{\text{TAM measurements}} \\ & + \underbrace{\frac{1}{2} \sum_{i=1}^{N-1} \left\| \omega_i^m - \hat{\omega}_i(\mathbf{q}_i, \mathbf{q}_{i+1}) - \beta_i \right\|_{W_v}^2}_{\text{gyro measurements}} \\ & + \underbrace{\frac{1}{2} \sum_{i=1}^{N-1} \left\| \beta_{i+1} - \beta_i \right\|_{W_u}^2}_{\text{bias random walk}} \end{aligned} \quad (46)$$

subject to

$$\mathbf{q}_i^T \mathbf{q}_i - 1 = 0, \quad \text{for all } i = 1, \dots, N \quad (47)$$

with $\hat{\omega}_i$ as computed in Eq. (44).

D. Solution Through Successive Linearization

At each iteration, this nonlinear least-squares problem is linearized around the current reference trajectory:

$$\mathbf{q}_i = \bar{\mathbf{q}}_i + \Delta \mathbf{q}_i \quad (48)$$

$$\beta_i = \bar{\beta}_i + \Delta \beta_i \quad (49)$$

to yield an unconstrained linear least-squares problem that can be solved with one matrix factorization. The linearized cost function is

$$\begin{aligned} \text{minimize} \quad & \frac{1}{2} \left\| \begin{matrix} \mathbf{q}_1^{(-)} \\ \beta_1^{(-)} \end{matrix} - \begin{matrix} \bar{\mathbf{q}}_1 \\ \bar{\beta}_1 \end{matrix} - \Delta \mathbf{q}_1 \right\|_{W_a}^2 + \frac{1}{2} \sum_{i=2}^N \left\| \mathbf{b}_i^m - \bar{\mathbf{b}}_i - \frac{\partial \mathbf{b}_i}{\partial \mathbf{q}_i} \Delta \mathbf{q}_i \right\|_{W_m}^2 \\ & \Delta \beta_1, \dots, \Delta \beta_N \\ & + \frac{1}{2} \sum_{i=1}^{N-1} \left\| \omega_i^m - \bar{\omega}_i(\bar{\mathbf{q}}_i, \bar{\mathbf{q}}_{i+1}) - \bar{\beta}_i - \frac{\partial \omega_i}{\partial \mathbf{q}_i} \Delta \mathbf{q}_i - \Delta \beta_i - \frac{\partial \omega_i}{\partial \mathbf{q}_{i+1}} \Delta \mathbf{q}_{i+1} \right\|_{W_v}^2 \\ & + \frac{1}{2} \sum_{i=1}^{N-1} \left\| \bar{\beta}_{i+1} + \Delta \beta_{i+1} - \bar{\beta}_i - \Delta \beta_i \right\|_{W_u}^2 \end{aligned} \quad (50)$$

subject to

$$\bar{\mathbf{q}}_i^T \bar{\mathbf{q}}_i - 1 + 2 \bar{\mathbf{q}}_i^T \Delta \mathbf{q}_i = 0, \quad \text{for all } i = 1, \dots, N \quad (51)$$

The nontrivial partial derivatives are

$$\frac{\partial \mathbf{b}_i}{\partial \mathbf{q}_i} = \left[\frac{\partial A(\mathbf{q}_i)}{\partial \mathbf{q}_1} \mathbf{r}_i \quad \frac{\partial A(\mathbf{q}_i)}{\partial \mathbf{q}_2} \mathbf{r}_i \quad \frac{\partial A(\mathbf{q}_i)}{\partial \mathbf{q}_3} \mathbf{r}_i \quad \frac{\partial A(\mathbf{q}_i)}{\partial \mathbf{q}_4} \mathbf{r}_i \right] \quad (52)$$

$$\frac{\partial \omega_i}{\partial \mathbf{q}_i} = -\frac{2}{\Delta T} \Xi^T(\mathbf{q}_{i+1}) \quad (53)$$

$$\frac{\partial \omega_i}{\partial \mathbf{q}_{i+1}} = \frac{2}{\Delta T} \Xi^T(\mathbf{q}_i) \quad (54)$$

where the partial derivatives in Eq. (52) can be computed from Eq. (34). In the cost function, $\bar{\mathbf{b}}_i$ is the (estimated) reference vector as seen in the spacecraft body frame, given by

$$\bar{\mathbf{b}}_i = A(\bar{\mathbf{q}}_i) \mathbf{r}_i \quad (55)$$

After each iteration, the reference quaternion trajectory is updated using Eqs. (48) and (49) for each time step in the horizon. The cost function is linearized around this new reference trajectory for a next iteration until convergence or a maximum number of iterations is reached. As a convergence criterion, it is here suggested to use a threshold on the KKT tolerance [32]. Note that, in this example, the RTI implementation for MHE is not used, but rather a fully converged MHE is implemented. An upper bound on the number of iterations is added to ensure real-time feasibility.

E. Results of Numerical Simulation

The MEKF, UKF, PF, and MHE algorithms are tested in a realistic example. An earth-pointing spacecraft in a circular orbit with 350 km altitude and inclination of 35 deg is considered. The three-axis magnetometer is sampled at 1 s intervals with a zero-mean white Gaussian noise with a standard deviation of 50 nT. The gyroscopes have the following noise characteristics: $\sigma_v = 0.3 \mu\text{rad/s}^{1/2}$ and $\sigma_u = 3.0 \times 10^{-4} \mu\text{rad/s}^{3/2}$. All filters are initialized with a 120 deg attitude estimation error and with an estimated bias vector of $[0, 0, 0]^T$. All filters are tuned with the real process and measurement noise covariances. The particle filter uses 1500 particles and implements an importance resampling at each time step to avoid particle degeneracy. Further sample diversity improvement is achieved by introducing a regularization step [8] that adds some

“jitter” to the particles using a Gaussian kernel. The MHE uses a horizon of 25 steps and limits the maximum number of Gauss–Newton iterations to 10. These numbers are chosen empirically to produce good results on this example problem. Figure 2 shows the result of a simulation run with a small initial gyro bias error equal to 50 deg/h in each axis. In this figure, the rss of the roll, pitch, and yaw estimation errors is plotted to show the overall performance of the different filters. All filters converge to the correct attitude. However, the UKF is better able to capture the nonlinearities in the model than the MEKF, and thus converges faster than the MEKF. The MHE converges faster than the MEKF and UKF, and the PF shows the fastest convergence in this example. All filters were compiled from C code and were run on a 2.67 GHz quad-core desktop computer with 4 GB of RAM memory. In this setup, the computation time for the MHE was approximately four to five times higher than that of the MEKF, whereas the computation time for the PF was approximately 1000 times more. However, this is highly dependent on the implementation method and computer language used. Note that, for small estimation errors, the effect of the nonlinearities becomes insignificant, and the MEKF, UKF, PF, and MHE solutions are almost equal.

When the initial gyro bias error is increased to 1000 deg/h, the MEKF is not able to find a correct attitude solution, and estimation errors remain close to 180 deg. One simulation run is shown in Fig. 3. The UKF does converge to the correct solution after some orbits. The PF and MHE exhibit a fast convergence, and both clearly outperform the two Kalman filters. These results are entirely in accordance with the performance of the MEKF and UKF published by Crassidis et al. in [6] and the performance of the particle filter published by Cheng and Crassidis in [9]. In the simulation run shown in Fig. 3, the MHE converges faster than the PF. However, it was not the objective of this research to find the optimal tuning parameters of the PF. The computation time for the MHE is about 200 times shorter than the computation time for the PF.

The MHE algorithm clearly exhibits a fast convergence on this example problem, at a computational complexity that allows onboard implementation. This could be implemented on a low-cost mission, for example, where only two sensors would be required, or this could serve as a safe mode for other spacecraft in case other sensors suffer failure or are switched off to preserve power.

IV. In-Flight Sensor Calibration

Though in widespread use, the simple gyro model presented in the previous section is insufficient in practical applications for high-accuracy spacecraft pointing. Gyroscope scale factor errors and sensor nonorthogonality can significantly limit the performance of the state estimator. This section first describes a star tracker model and a more advanced gyrosensor model that includes misalignment and scale factor errors as calibration parameters. A moving horizon estimator is developed to allow joint estimation of the attitude and

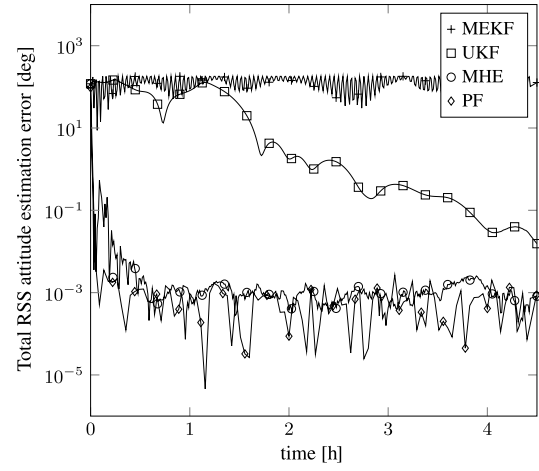


Fig. 3 Root sum squares estimation error for three different filters with large initial gyro bias: $\beta_0 = 1000$ deg/h.

bias states and the gyro calibration parameters. The moving horizon estimator is compared with different Kalman filters. The spacecraft is assumed to have two onboard sensors: a star tracker and a gyroscope. A simple star tracker measurement model is given by

$$\mathbf{q}^m = \delta \mathbf{q} \otimes \mathbf{q} \quad (56)$$

where $\delta \mathbf{q}$ is the measurement noise represented by a small angle quaternion. For small errors, $\delta \mathbf{q}$ should approach the zero-rotation quaternion $[0, 0, 0, 1]^T$. A first-order approximation of the error quaternion is

$$\delta \mathbf{q} \approx \begin{bmatrix} \delta \phi/2 \\ \delta \theta/2 \\ \delta \psi/2 \\ 1 \end{bmatrix} \quad (57)$$

with $\delta \phi$, $\delta \theta$, and $\delta \psi$ as the roll, pitch, and yaw measurement errors, respectively. A (nonlinear) gyro measurement model that includes sensor misalignment and scale factor errors is given by [12]

$$\omega_k^m = \omega_k + \beta_k - R \delta_p + \eta_k \quad (58)$$

where ω_k^m is the gyro output, ω_k is the real angular velocity, β_k is the gyro bias, and η_k is the gyro noise. In this equation, δ_p is a vector containing nine gyro calibration parameters: $\delta_p = [\lambda_x, \delta_{yz}, \delta_{zy}, \delta_{xz}, \lambda_y, \delta_{zx}, \delta_{xy}, \delta_{yx}, \lambda_z]^T$. The parameters λ_i denote the scale factors for each axis i , and the parameters $\delta_{i,j}$ denote the nonorthogonality angles between two axes i and j . The matrix R is then

$$R = \begin{bmatrix} \omega_x & \omega_y & \omega_z & 0 & 0 & 0 & 0 & 0 & 0 \\ 0 & 0 & 0 & \omega_x & \omega_y & \omega_z & 0 & 0 & 0 \\ 0 & 0 & 0 & 0 & 0 & 0 & \omega_x & \omega_y & \omega_z \end{bmatrix} \quad (59)$$

The nonlinear MHE problem is then

$$\begin{aligned} & \underset{\mathbf{q}_1, \dots, \mathbf{q}_N}{\text{minimize}} \quad \frac{1}{2} \left\| \mathbf{q}_1^{(-)} - \mathbf{q}_1 \right\|^2 \\ & \quad \underset{\beta_1, \dots, \beta_N}{\text{minimize}} \quad \underbrace{\left\| \beta_1^{(-)} - \beta_1 \right\|^2}_{\text{arrival cost}} \\ & \quad \underset{\delta_{p,1}, \dots, \delta_{p,N}}{\text{minimize}} \quad \underbrace{\frac{1}{2} \sum_{i=2}^N \left\| E(\mathbf{q}_i^m) \mathbf{q}_i - [0, 0, 0, 1]^T \right\|_{W_{\text{str}}}^2}_{\text{Star Tracker (STR) measurements}} \end{aligned} \quad (60)$$

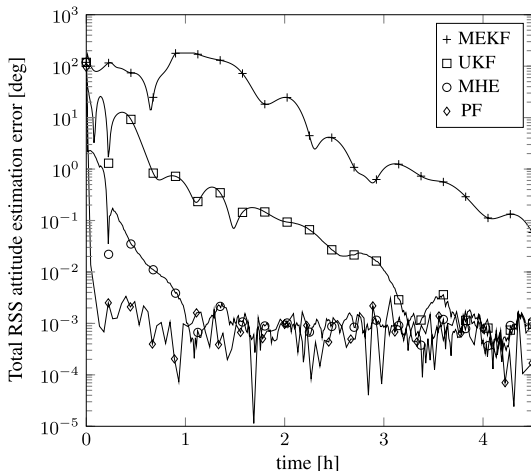


Fig. 2 Root sum squares estimation error for three different filters with small initial gyro bias: $\beta_0 = 50$ deg/h.

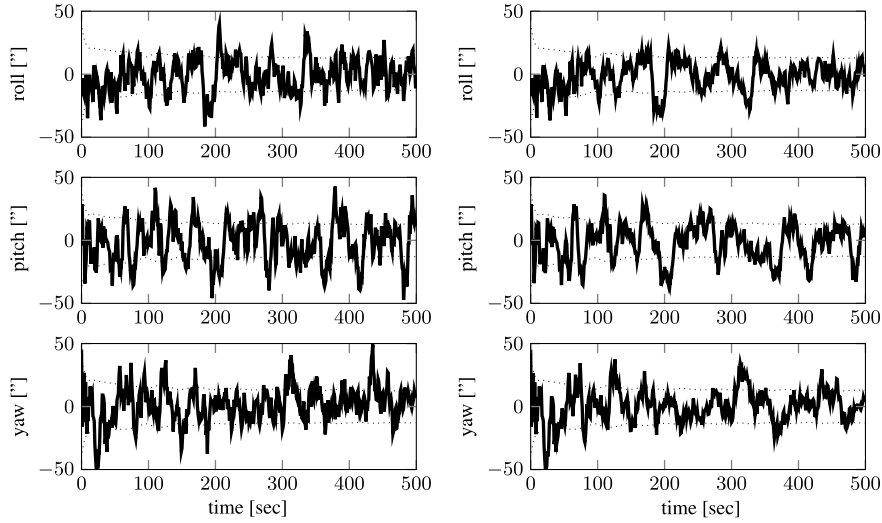


Fig. 4 Attitude estimation error (solid line) and $\pm 1\sigma$ error bounds (dotted line), using star tracker and gyro measurements: AKF (left figure) and MHE (right figure).

$$+\frac{1}{2}\sum_{i=1}^{N-1}\left\|\omega_i^m - \beta_i + R\delta_{pi} - \hat{\omega}_i\right\|_{w_v}^2 \quad (61)$$

Gyroscope (GYR) measurements

$$+\frac{1}{2}\sum_{i=1}^{N-1}\left\|\beta_{i+1} - \beta_i\right\|_{w_u}^2 \quad (62)$$

bias random walk

subject to

$$q_i^T q_i - 1 = 0, \quad \text{for all } i = 1, \dots, N \quad (63)$$

$$\delta_{pi+1} - \delta_{pi} = 0, \quad \text{for all } i = 1, \dots, N-1 \quad (64)$$

Note that the time dependence for the calibration parameters could be removed because they are constant in time. However, this would lead to a KKT matrix that does not have a band structure. Rather, the parameter vector is introduced at each time step, with the explicit constraint that this vector must remain constant in time. This nonlinear cost function is then linearized at each iteration step about the previous solution (or best estimate if no previous solution is available). This constrained optimization problem can then be solved using the iterative Gauss–Newton scheme described in Sec. II. For this problem, an RTI MHE has been implemented, as described in Sec. II, which limits the computational burden to one single Gauss–Newton iteration per time step. A horizon length of 20 time steps is selected empirically to produce good results on this example problem. The different filters are tested in a numerical simulation that is representative of a scientific spacecraft. Nominally, the payload is pointed at an inertial-fixed target. A calibration maneuver is performed to determine the gyro misalignment angles and scale factors. The calibration maneuver consists of a 0.5 deg/s sinusoid with periods of 100, 120, and 125 s in the x , y , and z axes, respectively. The gyro noise covariance is $\sigma_v = 1.4 \mu\text{rad/s}^{1/2}$, the

gyro bias random walk is $\sigma_u = 1.3 \mu\text{rad/s}^{3/2}$, the star tracker accuracy is 0.01 deg in each axis, and the calibration parameters are assumed constant over time with initial values $\lambda = 5000$ ppm and $\delta = 0.5$ deg in each axis. The star tracker is sampled at 1 Hz. When the basic six-state extended Kalman filter formulation (as described in Sec. III) and calibration parameters are neglected, the performance of the Kalman filter is greatly reduced, even to the point where the estimation error of the filtered output is larger than the error of the raw star tracker measurements. In [12], an alignment Kalman filter (AKF) is developed. In this Kalman filter, the state vector is augmented to include the nonorthogonality and scale factor parameters.

The attitude estimation errors for the AKF and the MHE at the final time are shown in Fig. 4. The MHE has a reduced attitude estimation error with respect to the AKF. The rms attitude estimation error over the entire simulation interval is given in Table 1. The increase in accuracy of the MHE over the other filters is clear from this table. Figure 5 shows the real and estimated scale factors for both the AKF and MHE. Because the MHE works over a batch of measurements, the MHE results in a more accurate attitude estimation than the Kalman filter, as quantified in Table 1. The estimation error for the nonorthogonality parameters shows a similar profile as the scale factor parameters. Note that, when a horizon length of $N = 2$ is used in the MHE, the estimated states and parameters are exactly equal to the estimated states in the AKF. If the horizon length is increased, the performance is better than the AKF. In this simulation, a horizon length of $N = 30$ is used. All filters were compiled from C code, and run on a 2.67 GHz quad-core desktop computer with 4 GB of RAM memory. In this setup, the computation time for the MHE was between two and five times longer than the computation time of the AKF in this simulation. Again, this highly depends on the implementation method and computer language.

V. Conclusions

The moving horizon estimation (MHE) method for optimal estimation of nonlinear dynamic systems is presented. The MHE problem is given as a least-squares objective function subject to constraints. With only equality constraints present, an efficient solution method based on a constrained Gauss–Newton approach is developed. By reordering the estimated states and Lagrange multipliers over the horizon, a sparse band structure can be obtained. This structure can then be exploited by using efficient numerical algorithms to factorize the Karush–Kuhn–Tucker matrix. By including a batch of measurements in the objective function, moving horizon estimation is expected to yield a better performance than Kalman filtering for nonlinear systems or systems that are not observable from one measurement. This is verified with applications to spacecraft attitude determination from vector observations and to

Table 1 Comparison of rms attitude estimation error for the different filters, with joint estimation of gyro calibration parameters

Filter	Root mean square estimation error, arcsec (1 arcsec = 1/3600 of a degree of arc)
STR	62
AKF	31
MHE	24

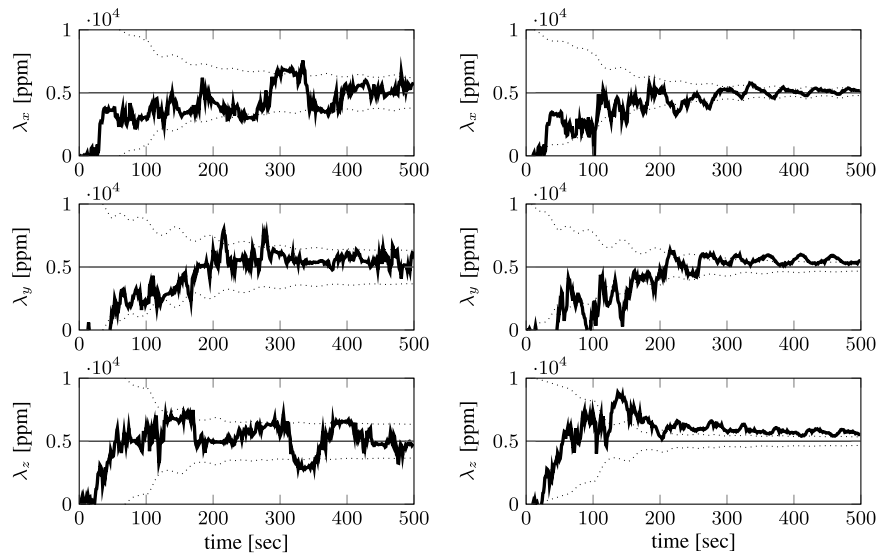


Fig. 5 Scale factor estimation error (solid line) and $\pm 1\sigma$ error bounds (dotted line), using star tracker and gyro measurements: AKF (left figure) and MHE (right figure).

joint attitude estimation and sensor calibration. In both examples, the performance of MHE is better than Kalman filtering and comparable to particle filtering, with a computational cost that is only four to five times higher than Kalman filtering and at least an order-of-magnitude faster than particle filtering.

Acknowledgments

The research leading to these results has received funding from the European Research Council (ERC) under the European Community's Seventh Framework Programme (FP7/2007–2013)/ERC grant agreement 227224 (PROSPERITY) and from the Fund for Scientific Research of Flanders (FWO), Belgium (G.0410.09).

References

- [1] Lefferts, E., Markley, F., and Shuster, M., "Kalman Filtering for Spacecraft Attitude Estimation," *Journal of Guidance, Control, and Dynamics*, Vol. 5, No. 5, 1982, pp. 417–429. doi:10.2514/3.56190
- [2] Markley, F., "Attitude Error Representations for Kalman Filtering," *Journal of Guidance, Control, and Dynamics*, Vol. 26, No. 2, 2003, pp. 311–317. doi:10.2514/2.5048
- [3] Crassidis, J., Markley, F., and Cheng, Y., "Survey of Nonlinear Attitude Estimation Methods," *Journal of Guidance, Control, and Dynamics*, Vol. 30, No. 1, 2007, pp. 12–28. doi:10.2514/1.22452
- [4] Psiaki, M., Martel, F., and Pal, P., "Three-Axis Attitude Determination via Kalman Filtering of Magnetometer Data," *Journal of Guidance, Control, and Dynamics*, Vol. 13, No. 3, 1989, pp. 506–514. doi:10.2514/3.25364
- [5] Vathsala, S., "Spacecraft Attitude Determination Using a Second-Order Nonlinear Filter," *Journal of Guidance, Control, and Dynamics*, Vol. 10, No. 6, 1987, pp. 559–566. doi:10.2514/3.20256
- [6] Crassidis, J., Markley, F., and Cheng, Y., "Unscented Filtering for Spacecraft Attitude Estimation," *Journal of Guidance, Control, and Dynamics*, Vol. 26, No. 4, 2003, pp. 536–542. doi:10.2514/2.5102
- [7] Coté, J., Kron, A., de Lafontaine, J., Naudet, J., and Santandrea, S., "PROBA-2 Attitude and Orbit Control System: In-Flight Results of AOCS Flight Experiments," *Proceedings of the Eighth International ESA Conference on Guidance, Navigation, and Control Systems*, The European Space Agency (ESA), Noordwijk, The Netherlands, 2011, pp. 1–19.
- [8] Ristic, B., Arulampalam, S., and Gordon, N., *Beyond the Kalman Filter — Particle Filters for Tracking Applications*, Artech House, London, 2004, pp. 35–62.
- [9] Cheng, Y., and Crassidis, J., "Particle Filtering for Attitude Estimation Using a Minimal Local-Error Representation," *Journal of Guidance, Control, and Dynamics*, Vol. 33, No. 4, 2010, pp. 1305–1310. doi:10.2514/1.47236
- [10] Shuster, M. D., Pitone, D. S., and Bierman, G. J., "Batch Estimation of Spacecraft Sensor Alignments—Relative Alignment Estimation," *Journal of Astronautical Sciences*, Vol. 39, No. 4, 1991, pp. 519–546.
- [11] Pittelkau, M., "Survey of Calibration Algorithms for Spacecraft Attitude Sensors and Gyros," *Advances in the Astronautical Sciences*, Vol. 129, No. AAS 07-295, 2008, pp. 651–706.
- [12] Pittelkau, M., "Kalman Filtering for Spacecraft System Alignment Calibration," *Journal of Guidance, Control, and Dynamics*, Vol. 24, No. 6, 2001, pp. 1187–1195. doi:10.2514/2.4834
- [13] Rauch, H., Tung, F., and Striebel, C., "Maximum Likelihood Estimates of Linear Dynamic Systems," *Journal of Guidance, Control, and Dynamics*, Vol. 3, No. 8, 1965, pp. 1445–1450. doi:10.2514/3.3166
- [14] Moore, J., "Discrete-Time Fixed-Lag Smoothing Algorithms," *Automatica*, Vol. 9, No. 2, 1973, pp. 163–173. doi:10.1016/0005-1098(73)90071-X
- [15] Elliot, R., and Moore, J., "State and Parameter Estimation for Linear Systems," *Journal of Mathematical Systems, Estimation, and Control*, Vol. 6, No. 1, 1996, pp. 125–128.
- [16] Moore, J., and Teo, K., "Smoothing as an Improvement on Filtering in High Noise," *Systems and Control Letters*, Vol. 8, No. 1, 1986, pp. 51–54. doi:10.1016/0167-6911(86)90029-0
- [17] Moore, J., and Tam, P., "Fixed-Lag Smoothing for Nonlinear Systems with Discrete Measurements," *Information Sciences*, Vol. 6, 1973, pp. 151–160. doi:10.1016/0020-0255(73)90032-7
- [18] Davis, S., and Lai, J., "Attitude Sensor Calibration for the Ocean Topography Experiment Satellite," *Proceedings of the SPIE Space Guidance, Control, and Tracking Conference*, Vol. 1949, 1993, pp. 80–91. doi:10.1117/12.157073
- [19] Shuster, M. D., "A Simple Kalman Filter and Smoother for Spacecraft Attitude," *Journal of Astronautical Sciences*, Vol. 37, No. 1, 1989, pp. 89–106.
- [20] Sedlak, J., "Comparison of Kalman Filter and Optimal Smoother Estimates of Spacecraft Attitude," NASA TR-N94-35638, 1994, pp. 431–445.
- [21] Ohtsuka, T., and Fujii, H., "Nonlinear Receding Horizon Estimation by Real-Time Optimization Technique," *Journal of Guidance, Control, and Dynamics*, Vol. 19, No. 4, 1996, pp. 863–870. doi:10.2514/3.21711
- [22] Rao, C. V., Rawlings, J. B., and Mayne, D. Q., "Constrained State Estimation for Nonlinear Discrete-Time Systems: Stability and Moving Horizon Approximations," *IEEE Transactions on Automatic Control*,

- Vol. 48, No. 2, 2003, pp. 246–258.
doi:10.1109/TAC.2002.808470
- [23] Tenny, M., and Rawlings, J., “Efficient Moving Horizon Estimation and Nonlinear Model Predictive Control,” *Proceedings of the American Control Conference*, IEEE, 2002, pp. 4475–4480.
- [24] Valdez-Gonzalez, H., Flaus, J., and Ancuna, G., “Moving Horizon State Estimation with Global Convergence Using Interval Techniques: Applications to Biotechnological Processes,” *Journal of Process Control*, Vol. 13, No. 4, 2003, pp. 325–336.
doi:10.1016/S0959-1524(02)00060-4
- [25] Jorgensen, J., Rawlings, J., and Jorgensen, S., “Numerical Methods for Large-Scale Moving Horizon Estimation and Control,” *Proceedings of the International Symposium on Dynamics and Control of Process Systems (DYCOPS)*, International Federation of Automatic Control (IFAC) Paper 149, 2004.
- [26] Kang, W., “Moving Horizon Numerical Observers of Nonlinear Control Systems,” *IEEE Transactions on Automatic Control*, Vol. 51, No. 2, 2006, pp. 344–350.
doi:10.1109/TAC.2005.863509
- [27] Zavala, V., Laird, C., and Biegler, L., “A fast Computational Framework for Large-Scale Moving Horizon Estimation,” *Proceedings of the Eighth International Symposium on Dynamics and Control of Process Systems*, International Federation of Automatic Control (IFAC) Paper 1, 2007.
- [28] Kühl, P., Diehl, M., Kraus, T., Schlöder, J., and Bock, H., “A Real-Time Algorithm for Moving Horizon State and Parameter Estimation,” *Computer and Chemical Engineering*, Vol. 35, No. 1, 1996, pp. 71–83.
doi:10.1016/j.compchemeng.2010.07.012
- [29] Diehl, M., Ferreau, H., and Haverbeke, N., “Efficient Numerical Methods for Nonlinear MPC and Moving Horizon Estimation,” *Nonlinear Model Predictive Control*, Springer-Verlag, Berlin, 2009, pp. 391–417.
- [30] Haverbeke, N., “Efficient Numerical Methods for Moving Horizon Estimation,” Ph.D. Thesis, Katholieke Universiteit Leuven, Leuven, Belgium, 2011, pp. 82–87.
- [31] Bock, H., Kostina, E., and Schlöder, J., “Numerical Methods for Parameter Estimation in Nonlinear Differential Algebraic Equations,” *GAMM Mitteilungen*, Vol. 30, No. 2, 2007, pp. 376–408.
doi:10.1002/gamm.200790024
- [32] Nocedal, J., and Wright, S., *Numerical Optimization*, Springer, New York, 2000, pp. 392–418.
- [33] Wertz, J. R., *Spacecraft Attitude Determination and Control*, Springer-Verlag, New York, NY, 1978, pp. 410–459.
- [34] Marsden, J. E., and West, M., “Discrete Mechanics and Variational Integrators,” *Acta Numerica*, Vol. 10, 2001, pp. 357–514.
doi:10.1017/S096249290100006X